Title: Nuclear polymorphism and non-proliferative adult neurogenesis in human neural crest-derived cells.

Authors: Carlos Bueno[1,*], Marta Martínez-Morga[2] and Salvador Martínez[1].

[1] Instituto de Neurociencias de Alicante (UMH-CSIC), San Juan, Alicante, 03550, Spain.

[2] Department of Human Anatomy and Institute of Biomedical Research (IMIB), University of Murcia, Faculty of Medicine, Murcia, 30800, Spain.

***Corresponding author**: Carlos Bueno, PhD., Instituto de Neurociencias de Alicante. UMH-CSIC, Campus de San Juan, E-03550-Alicante, Spain. Tel.: 0034-96-591-9556. Fax: 0034-96-591-9555. E-mail: cbueno@umh.es

Summary

Self-renewal and lineage regulation of neural stem cells in the adult mammalian brain (aNSCs) are still far from been understood. Although previous studies have reported that some aNSCs in neurogenic niches showed irregular nuclei, their functional significance remains elusive. We used neural crest-derived human periodontal ligament stem cells (hPDLSCs) as an *in vitro* cell-model of neurogenesis to investigate the functional significance of nuclear polymorphisms. We observed that hPDLSCs-derived neurons are not generated through cell division from stem cells, the cell shape is reset and they begin their neuronal differentiation as rounded spheres. Moreover, transient nuclear lobulation coincident with neurogenesis was also observed. Our results provide evidence that these dynamic structural events may also occur in neurogenic niches. Finally, we show that hPDLSCs-derived neurons and neuronal cultures derived from rodent brains present a similar pattern of polarity formation, demonstrating that is possible to reproduce neurogenic processes and obtain neurons from hPDLSCs.

Introduction

Neural stem cells (NSCs) are multipotent populations of undifferentiated cells present both during development and in the adult central nervous system that give rise to new neurons and glia (Conti and Cattaneo., 2010). The self-renewal and multipotent properties demonstrated by NSC *in vitro* (Reynolds and Weiss., 1992) have not been clearly demonstrated *in vivo*. (Gabay et al., 2003; Suh et al., 2007; Conti and Cattaneo., 2010; Bond et al., 2015).

The presence of neural stem cells in the adult mammalian brain (aNSCs) have been described in two neurogenic niches, the ventricular-subventricular zone (V-SVZ) of the anterolateral ventricle wall (Doetsch et al., 1997; Doetsch et al., 1999) and the subgranular zone (SGZ) of the hippocampal dentate gyrus (Seri et al., 1999; Seri et al., 2001; Filippov et al., 2003; Fukuda et al., 2003).

The study of the cell composition of neurogenic niches and the use of methods for detecting proliferating cells, suggest that neurogenesis occurs progressively through sequential phases of proliferation and the neuronal differentiation of aNSCS. In the V-SVZ, putative aNSCs (type B cells) divide to give rise to intermediate progenitor cells (type C cells), which in turn generate polarized neuroblasts (type A cells). The neuroblast then migrate into the olfactory bulb and differentiate into distinct types of neurons. In the SGZ, putative aNSCs (type 1 cells) divide to give rise to intermediate progenitor cells (type-2 cells) which exibit limited rounds of proliferation before generating polarized neuroblast (type-3 cells). Neuroblast, as polarized cells, then migrate, guided by the leading process, along SGZ and differentiate into dentate granule neurons (Fuentealba., 2012; Bond et al., 2015).

Ultrastructure and immunocytochemistry studies show that the V-SVZ stem cell niche contains cells with irregular (polymorphic) nuclei. Type-B cells have irregular nuclei that frecuently contain invaginations. Type-C cells nuclei contain deep invaginations and Type-A cell nuclei are also occasionally invaginated (Doetsch et al., 1997). Futhermore, recent studies have shown that murine and human V-SVZ have segmented nuclei connected by an internuclear bridge (Guerrero-Cázares et all., 2011; Capilla-Gonzalez et al., 2014; Cebrián-Silla et al., 2017). Although it has been suggested that these are associated with quiescence in aNSCs (Cebrián-Silla et al., 2017), the functional significance of different nuclear morphologies remains elusive.

In adittion, how neuroblasts acquire the appropriate cell polarity to initiate their migration remains unclear (Ghashghaei et al., 2007). The process of neuronal polarization has been studied for decades using dissociated rodent embryonic hippocampal pyramidal neurons and postnatal cerebellar granule neurons in culture (Tahirovic and Bradke., 2009; Takano et al., 2015). During neuronal polarization *in vitro*, the morphological changes in cultured neurons are divided into different stages.

Upon isolation, dissociated pyramidal neurons retract their processes, so that their development *in vitro* begins as rounded spheres that spread lamellipodia (stage 1). These spheres appear symmetrical, extending and retracting several immature neurites of a similar length (stage 2). Elongation of a single process, that which presumably becomes the axon, breaks this symmetry (stage 3). The next step involves the remaining short neurites morphologically developing into dendrites (stage 4) and the functional polarization of axon and dendrites (stage 5), including dendritic spine and synapse formation (Dotti et al., 1988). Dissociated granule neurons also present a lamellipodia after attaching to the substratum (stage 1). These spheres extend a unipolar process at a single site on the plasma membrane (stage 2) followed by extension of a second process from the opposite side of the cell body, resulting in a bipolar morphology (stage 3). One of the two axon elongates futher and start branching (stage 4), and shorter dendritic processes develop around the cell body (stage 5) (Powell et al., 1997).

Understanding the sequence of events from aNSCs to neuron is not only important for the basic knowledge of NSCs biology, but also for therapeutic applications (Casarosa et al., 2014). The major barrier to studying human aNSCs is the inaccessibility of living tissue, therefore an enormous effort has been made in this study to derive neurons from human stem cells (Goldman., 2016). *In vitro* models of adult neurogenesis mainly utilize fetal, postnatal and adult NSCs (Azari and Reynolds., 2016). Neural crest stem cells (NCSCs) are a migratory cell population that generate numerous cell lineages during development, including neurons and glia (Bronner-Fraser., 1995; Crane and Trainor., 2006). NCSCs are present not only in the embryonic neural crest, but also in various neural crest-derived tissues in the fetal and even adult organs (Achilleos and Trainor., 2012). The periodontal ligament is a connective tissue surrounding the tooth root that contains a source of human NCSCs which can be accessed with minimal technical requirements and little inconvenience to the donor. (Liu and Cheung., 2016).

In previous publication, we showed that several stem cell and neural crest cell markers are expressed in human adult periodontal ligament (hPDL) tissue and hPDL-derived cells. *In vitro*, hPDL-derived cells differentiate into neural-like cells based on cellular morphology and neural marker expression. *In vivo,* hPDL-derived cells survive, migrate and expressed neural markers after being grafted to the adult mouse brain. Moreover, some hPDL-derived cells graft into stem cell niches such as V-SVZ of the anterolateral ventricle wall and the SGZ of the dentate gyrus in the hippocampus. The hPDL-derived cells located in the stem cell niches show neural stem morphology (Bueno et al., 2013). Therefore, the neural crest origin and neural potential make human periodontal ligament stem cells (hPDLSCs) interesting as an *in vitro* human cell model of neurogenesis for investigating aNSCs to neuron differentiation mechanisms.

Here, we show that hPDLSCs-derived neurons are not directly generated through cell division from stem cells. In fact, the cell shape of neural precursors is reset and start their neuronal development as round spheres. To our knowledge, this article provides the first observation of these morphological events during *in vitro* neurogenesis and neuron polarization in human aNCSCs, and we have discovered a transient cell nuclei lobulation coincident to *in vitro* neurogenesis, without being related to cell proliferation. Morphological analysis also reveals that the V-SVZ of the anterolateral ventricle wall and the SGZ of the hippocampal dentate gyrus in the adult mouse brain contains cells with nuclear shapes highly similar to those observed during *in vitro* neurogenesis from hPDLSCs, suggesting that neuronal differentiation from aNSCs may also occur during *in vivo* adult mammalian neurogenesis without being related to cell proliferation.

In addition, we demonstrate that hPDLSC-derived neurons and primary neuronal cultures derived from rodent brains show similar polarity formation patterns during neurogenesis, providing strong evidence that it is possible to reproduce neurogenic processes and obtain neurons from hPDLSCs. Thus, hPDLSCs could be used as an *in vitro* human cell-based model for neurogenesis and neuronal polarization.

Results

As noted in the introduction, the aim of this work was to evaluate the sequence of biological events occurring during the neural differentiation of hPDLSCs. Morphological characteristics of the hPDLSCs, including cell shape, cell surface features, cytoskeleton, and nuclear morphology were examined in cells under proliferation and neural differentiation conditions.

hPDLSCs cultured in basal media. Under proliferation conditions, hPDLSCs displayed a fibroblast-like morphology with low-density microvilli on the cell surface (Figure 1A) and actin microfilaments and β-III tubulin microtubules oriented parallel to the longitudinal axis of the cell (Figure 1B). The cytoskeletal protein class III beta-tubulin isotype is widely regarded as a neuronal marker in developmental neurobiology and stem cell research (Flynn., 2013). Dental and oral-derived stem cells displayed spontaneous expression of neural marker β-III tubulin, even without

having been subjected to neural induction (Foudah et al., 2014). Western blot analysis verified the expression of β-III tubulin in hPDLSCs (Figure 1C). Undifferentiated hPDL-derived cells displayed a flattened, ellipsoidal nucleus, often located in the center of the cell and with a nuclear volume around 925´356 ±52´6184 μm^3 (Figure 1D).

hPDLSCs cultured in neural induction media. After 14 days of neural differentiation conditions, the hPDLSCs displayed different morphologies, including round cells with small phase-bright cell bodies and short processes; highly irregulary-shaped cells; and, also, unipolar, bipolar and multipolar-shaped cells with small phase-bright cell bodies and multiple branched processes (Figure 1E). In addition, cells of different size were also observed (Figure 1F). Futhermore, microscopic analysis revealed that some hPDLSCs have different nuclear shapes, including lobed nuclei connected by an internuclear bridge (Figure 1G). The results indicate that the cell culture simultaneously contains hPDLSCs at different stages of neurogenesis and neuronal polatization. We acknowledge that the definitive sequence of *in vitro* neurogenesis and neuronal polarization from hPDLSCs will be provided only by time-lapse microscopy of a single cell, but in our experimental conditions, several pieces of data suggest how these steps may occur.

***In vitro* neurogenesis from hPDLSCs**. After neural induction, hPDLSCs undergo a dramatic change in shape and size, first adopting highly irregular forms and then gradually contracting into round cells with small phase-bright cell bodies (Figure 2A). Cytoskeletal remodeling is observed during the morphological changes that occurred when the hPDLSCs round up to a near-spherical shape. Actin microfilament not longer surround the nucleus and became cortical. Unlike actin, β-III tubulin seems to accumulate around the nucleus (Figure 2B). Actin microfilament and β-III tubulin microtubule network are almost lost in the rounded cells (Figure 2C). Scanning electron micrographs show that hPDLSCs also experience dramatic changes in cell surface features. Under proliferation conditions, hPDLSCs remain very flat, presenting low-density microvilli on their surface, but there is a marked increase in the number of microvilli as the cells round up to near-spherical shape (Figure 3D). The surface of the round cells is almost devoid of microvilli (Figure 3E).

Neuronal polarization of hPDLSCs-derived neurons. Morphological analysis revealed that hPDLSCs-derived neurons display a sequence of morphologic development highly similar to those observed in dissociated-cell cultures prepared from rodent brain (Figures 3-5). hPDLSCs-derived neurons also start their development as rounded spheres that initiated neurite outgrowth at a single site on the plasma membrane, first becoming unipolar, stages 1-2 (Figure 3A). We did not observe the development of lamellipodia around the circumference of the cell body. These unipolar cells, later transformed into cells containing several short neurites, developed around the cell body, stage 3 (Figure 3B). An analysis of the cytoskeletal organization during spherical stages of hPDLSCs-derived neurons showed that the β-III microtubules and actin microfilament network is reorganized. Cytoskeletal protein β-III tubulin was densely accumulated under the cell membrane of the hPDLSCs-derived neurons cell bodies and in cell neurites (Figures 3A and 3B) while actin microfilaments were mainly found in cell neurites (Figure 3C). We observed that

hPDLSCs-derived neurons produce neurites that showed growth cone formations at their tips (Figure 3C-3D). The central domain of the growth cone contains β-III tubulin microtubules and the peripheral domain is composed of radial F-actin bundles (Figure 3D), similar to the typical spatial organization described in neurons (Foster and Smith, 1988; Blanquie and Bradke., 2018). Scanning electron micrographs also showed that the growth cone of hPDLSCs-derived neurons contained filopodia and vesicles on the cell surface (Figure 3E). These finding are consistent with a previous study reporting that membrane addition and extension in growth cones is mediated by diverse mechanism, including exocytosis of vesicular components (Ros et al., 2015).

At later stages of differentiation, the hPDLSCs-derived neurons gradually adopted a complex morphology by forming several processes, stage 4 (Figure 3F) that grew and arborized, adquiring dendritic-like and axonal-like identities, giving rise to a variety of neuron-like morphologies (Figure 3G). The next step, stage 5, in neuronal polarization from rodent neurons in culture is the functional polarization of axon and dendrites, including dendritic spine formation and axon branch formation. Dendritic spines are micron-sized dendrite membrane protrusions (Hering and Sheng., 2001). Depending on the relative sizes of the spine head and neck, they can be subdivided into different categories, including filopodium, mushroom, thin, stubby, and branched spines (von Bohlen Und Halbach., 2009). Dendritic spines are actin-rich compartments that protrude from the microtubule-rich dendritic shafts of principal neurons (Merriam et al., 2013). Based on morphology, complexity, and function, axon branching is grouped into different categories, including arborization, bifurcation, and collateral formation (Gibson and Ma., 2011).

Our morphological analysis revealed that hPDLSCs-derived neurons developed well-differentiated axonal-like and dendritic-like domains. These types of processes differ from each other in morphology (Figures 3H-4D). Cytoskeletal protein β-III tubulin and F-actin staining showed that the hPDLSCs-derived neurons comprised multiple branched dendrite-like processes with dendritic spines-like structures (Figure 3H). Scanning electron micrographs showed that the hPDLSCs-derived neurons also contained multiple branched dendrite-like processes with variously shaped spine-like protusions, highly similar to filopodium, mushroom, thin, stubby, and branched dendritic spines shapes (Figure 4A). Futhermore, hPDLSCs-derived neurons also displayed different types of axonal branch-like structures, including bifurcation (Figure 4B), arborization (Figure 4C), and collateral formation (Figure 4D).

The last step in neuronal polarization from rodent neurons in culture is synapse formation. The most frequent types of synaptic communication include axodendritic, axosomatic, axoaxonic and dendrodendritic synapses. Morphological analysis revealed that the hPDLSCs-derived neurons connected to one another (Figure 5A) through different types of synapse-like interactions, including dendrodendritic-like, axoaxonic-like and axodendritic-like synapses (Figure 5B). Synapse-associated proteins Cx43, Synaptophysin and Synapsin1 were found accumulated in the cell surface of neurites (Figure 5C).

Nuclear remodeling. As noted above, undifferentiated hPDL-derived cell displayed a flattened, ellipsoidal nucleus, often located in the center of the cell, and with a nuclear volume around 925´356 ±52´6184 μm^3 (Figure 1D). Morphological analysis revealed that nuclear remodeling, including nuclear shape, nuclear volume, and nuclear position within the cell, occurred during *in vitro* neurogenesis from hPDLSCs (Figure 6). We acknowledge that the definitive sequence of nuclear remodeling when hPDLSCs round up to near-spherical shape will only be provided by time-lapse microscopy, but our accumulated data suggests how these steps may occur.

The nucleus located in the center of the cell start to move towards an asymmetrical position within the cell (Figure 6A-6I). This nuclear movement is accompanied by the transient formation of lobed nuclei connected by an internuclear bridge (Figure 6J-T). Finally, there is restoration of irregular, but non-lobed, nucleus with an eccentric position within hPDLSCs-derived neurons (Figure 6U-Z). Although it has been suggested that lobed nuclei connected by an internuclear bridge are associated with quiescence in aNSCs (Cebrián-Silla et al., 2017), we observed that this kind of nuclei is associated to nuclear movement within the cell during initial phases of neurogenesis, without being related to cell proliferation.

Interestingly, the morphological analysis revealed that the adult rodent V-SVZ of the anterolateral ventricle wall (Figure 7A) and the SGZ of the hippocampal dentate gyrus (Figure 7B), where adult neurogenesis has been clearly demonstrated, contained abundant cells with nuclear shapes highly similar to those observed during *in vitro* neurogenesis from hPDLSCs. No lobed nuclei were observed as PDL-derived neurons gradually acquired a more mature neuronal-like morphology (Figure 8A). We also found that as the cells round up to a near-spherical shape the nuclear volume of the hPDLSCs decreases to an approximate volume of 279´589±38´8905 μm^3 (Figure 8B). Mitotic chromosomes were not observed during the described of *in vitro* neurogenesis processes or neuronal polarization from hPDLSCs (Figures 6 and S1).

Discussion

In this study, we show that hPDLSCs-derived neurons are not directly generated through cell division from stem cells. The undifferentiated polygonal and fusiform cell shapes are reset and start their neuronal development as rounded spheres. To our knowledge, this article provides the first observations of these morphological events during *in vitro* neurogenesis and neuron polarization from human aNCSCs, and we have discovered a transient cell nuclei lobulation coincident to *in vitro* neurogenesis, without being related to cell proliferation. Morphological analysis also revealed that the adult rodent V-SVZ of the anterolateral ventricle wall, as well as the SGZ of the hippocampal dentate gyrus, where adult neurogenesis has been clearly demonstrated, contains cells with nuclear shapes highly similar to those observed during *in vitro* neurogenesis from hPDLSCs.

Previous ultrastructure and immunocytochemistry studies also show that the V-SVZ stem cell niche contains cells with different morphologies and irregular nuclei (Doetsch et al., 1997; Doetsch et al., 1999). Type-B cells have irregular nuclei that frecuently contain invaginations and irregular contours of the plasma membrane. Type-C cells nuclei contained deep invaginations and these cells are more spherical. Type-A cells have elongated cell body with one or two processes and the nuclei are occasionally invaginated. Futhermore, recent studies have shown that murine and human V-SVZ have segmented nuclei connected by an internuclear bridge (Guerrero-Cázares et al., 2011; Capilla-Gonzalez et al., 2014; Cebrián-Silla et al., 2017). In adittion, previous studies shown irregular shaped BrdU-positive nuclei in the adult SGZ (Kuhn et al., 1996; Urbach et al., 2008). Adult SGZ NSCs (type 1 cells) have irregular contours of the plasma membrane, and differences in heterochromatin aggregation has been also observed (Seri et al., 2001).

It has commonly been assumed that neurogenesis occurs progressively through sequential phases of proliferation (Fuentealba et al., 2012; Bond et al., 2015). Despite the advantages for the detection of neurogenesis using exogenosus thymidine analog administration or endogenous cell cycle markers, in addition to cell stage and lineage commitment markers, recent findings indicate that some observations interpreted as cell division could be normal DNA turnover or DNA repair (Sohur et al., 2006; Kuhn et al., 2016). Thymidine analogs such as tritiated thymidine and BrdU may also be incorporated during DNA synthesis that is not related to cell proliferation (Cameron et al., 1993; Palmer et al., 1995). Proliferating cell nuclear antigen is also invoved in DNA repair (Uberti et al., 2003). Positivity of the proliferation marker KI-67 in noncycling cells has also been observed (Van Oijen et al.,1998). In adittion, the self-renewal and multipotent properties demonstrated by NSC *in vitro* (Reynolds and Weiss., 1992) have not been clearly demonstrated *in vivo*. (Gabay et al., 2003; Suh et al., 2007; Conti and Cattaneo., 2010; Bond et al., 2015).

Taken together, these results suggest that the sequence of events from aNSCs to neuron may also occur without being related to cell proliferation. It would therefore be interesting to examine whether SVZ and SGZ intermediate progenitor cells represent different stages of neurogenesis without being related to cell proliferation.

Beyond the central nervous system, the presence of lobed nuclei has been reported in most blood and immune cells, but the functional significance of multilobed nuclear structures is not yet known (Carvalho et al., 2015; Georgopoulos., 2017). It would also be interesting to examine whether these putative madure cells also represent different stages of haematopoietic stem cell differentiation without being related to cell proliferation.

Futhermore hPDLSCs-derived neurons and dissociated-cell cultures prepared from rodent brains show similar phases in the of polarity formation process, providing strong additional evidence that it is possible to obtain neurons from hPDLSCs, as suggested by their neural-crest origin and stem cell characteristics (Bueno et al., 2013). Thus, hPDLSCs could be also used as an *in vitro* human cell-based model for neurogenesis and neuronal polarization (Azari and Reynolds., 2016).

Alterations in nuclear morphologies are closely associated with a wide range of human diseases, including muscular dystrophy and cancer (Gundersen and Worman., 2013). Thus, hPDLSCs could facilitate an understanding of the mechanisms regulating nuclear morphology in response to cell shape changes and their functional relevance (Dupin and Etienne-Manneville., 2011; Skinner and Johnson., 2017). In addition, the easy procedure for obtaining these from adults in normal or pathological condictions, may represent, as we have demonstrated with periodontal ligament cells from children (Jones et al., 2012; Quesada et al., 2015), a suitable way of developing *in vitro* cell models of human diseases. These results, together with our previously published data, show that the isolation and neural differentiation of hPDLSCs is a powerful tool in basic and translational research into the understanding of normal function and central nervous system disorders.

Acknowledgments

We greatly appreciate the technical assistance of Microscopy Section of the University of Murcia in preparing samples for scanning electron microscopy. This work was supported by the grants Institute of Health Carlos III (RD16/001/0010) and Spanish MICINN (SAF2014-59347-C2-1-R) and (SAF2017-83702-R).

Author contributions

C.B. is responsible for the conception and design, collection of data, data analysis and interpretation, and manuscript writing. M.M.M. is responsible for the collection of data. S.M is responsible for the conception and design, manuscript writing, and financial support.

References

Achilleos, A., and Trainor, P.A. (2012). Neural crest stem cells: discovery, properties and potential for therapy. Cell Res. *22*, 288-304.

Azari, H., and Reynolds, B.A. (2016). In vitro models for neurogenesis. *Cold Spring Harbour Perspectives in Biology.* vol. 8, no. 16.

Blanquie, O., and Bradke, F. (2018). Cytoskeleton dynamics in axon regeneration. Curr. Opin. Neurobiol*. 51*, 60-69.

Bond, A.M., Ming, G.L., and Song, H. (2015). Adult mammalian neural stem cells and neurogenesis: five decades later. Cell Stem Cell *17*, 385-395.

Bronner-Fraser, M. (1995). Origins and developmental potential of the neural crest. Exp. Cell Res. *218***,** 405-417.

Bueno, C., Ramirez, C., Rodríguez-Lozano, F.J., Tabarés-Seisdedos, R., Rodenas, M., Moraleda, J.M., Jones, J.R., and Martinez, S. (2013). Human adult periodontal ligament-derived cells integrate and differentiate after implantation into the adult mammalian brain. Cell Transplant. *22*, 2017-2028.

Cameron, H.A., Woolley, C.S., McEwen, B.S., and Gould, E. (1993). Differentiation of newly born neurons and glia in the dentate gyrus of the adult rat. Neuroscience. *56*, 337-344.

Capilla-Gonzalez, V., Cebrian-Silla, A., Guerrero-Cazares, H., Garcia-Verdugo, J.M., and Quiñones-Hinojosa, A. (2014). Age-related changes in astrocytic and ependymal cells of the subventricular zone. Glia *62*, 790-803.

Carvalho, L.O., Aquino, E.N., Neves, A.C., and Fontes, W. (2015). The neutrophil nucleus and its role in neutrophilic function. J. Cell. Biochem.*116*, 1831-1836.

Casarosa, S., Bozzi, Y., and Conti, L. (2014). Neural stem cells: ready for therapeutic applications? Mol. Cell. Ther. 2:31.

Cebrián-Silla A., Alfaro-Cervelló, C., Herranz-Pérez, V., Kaneko, N., Park, D.H., Sawamoto, K., Alvarez-Buylla, A., Lim, D.A., and García-Verdugo J.M. (2017). Unique organization of the nuclear envelope in the post-natal quiescent neural stem cells. Stem Cell Reports *9*, 203-216.

Conti, L., and E. Cattaneo, E. (2010). Neural stem cell systems: physiological players or in vitro entities? Nat. Rev. Neurosci. *11*, 176-87.

Crane, J. F., and Trainor, P.A. (2006). Neural crest stem and progenitor cells. Annu. Rev. Cell Dev. Biol. *22***,** 267–286.

Doetsch, F., Garcia-verdugo, J.M., and Alvarez-buylla, A. (1997). Cellular composition and three-dimensional organization of the subventricular germinal zone in the adult mammalian brain. J. Neurosci. *17***,** 5046-5061.

Doetsch, F., Caillé, I., Garcia-verdugo, J.M., and Alvarez-buylla, A. (1999). Subventricular zone astrocytes are neural stem cells in the adult mammalian brain. Cell *97***,** 703-716.

Dotti, C.G., Sullivan, C.A., and Banker, G.A. (1988). The establishment of polarity by hippocampal neurons in culture. J. Neurosci. *8*, 1454-1468.

Dupin, I., and Etienne-Manneville, S. (2011). Nuclear positioning: mechanisms and functions. Int. J. Biochem. Cell Biol. *43***,** 1698-16707.

Filippov V., Kronenberg, G., Pivneva, T., Reuter, K., Steiner, B, Wang, L.P., Yamaguchi, M., Kettenmann, H., and Kempermann, G. (2003). Subpopulation of nestin-expressing progenitor cells in the adult murine hippocampus shows electrophysiological and morphological characteristics of astrocytes. Mol. Cell Neurosci. *23*, 373-82.

Flynn, K.C. (2013). The cytoskeleton and neurite initiation. BioArchitecture *3*, 86-109.

Forscher, P., and Smith, S.J. (1988). Actions of Cytochalasins on the organization of actin filaments and microtubules in a neuronal growth cone. J. Cell Biol. *107*, 1505-1516.

Foudah, D., Monfrini, M., Donzelli, E., Niada, S., Brini, A.T., Orciani, M., Tredici, G., and Miloso, M. (2014). Expression of neural markers by undifferentiated mesenchymal-like stem cells from different sources. J. Immunol. Res*.,* vol. 2014, Article ID 987678.

Fuentealba, L.C., Obernier, K., and Alvarez-Buylla, A. (2012). Adult stem cells bridge their niche. Cell Stem Cell *6***,** 678-708.

Fukuda, S., Kato, F., Tozuka, Y., Yamaguchi, M., Miyamoto, Y., and Hisatsune, T. (2003). Two distinct subpopulations of nestin-positive cells in adult mouse dentate gyrus. J. Neurosci. *23*, 9357-9366.

Gabay, L., Lowell, S., Rubin, L. L., and Anderson, D. J. (2003). Deregulation of dorsoventral patterning by FGF confers trilineage differentiation capacity on CNS stem cells in vitro. Neuron *40*:485–499.

Georgopoulos, K. (2017). In search of the mechanism that shapes the neutrophil´s nucleus Genes Dev. *31*, 85-87.

Ghashghaei, H.T., Lai, C., and Anton, E.S. (2007). Neuronal migration in the adult brain: are we there yet? Nat. Rev. Neurosci. *8*, 141-151.

Gibson, D.A., and Ma, L. (2011). Developmental regulation of axon branching in the vertebrate nervous system. Development *138*, 183-195.

Goldman, S.A. (2016). Stem and progenitor cell-based therapy of the central nervous system: hopes, hype, and wishful thinking. Cell Stem Cell *18*, 174-88.

Guerrero-Cázares, H., Gonzalez-Perez, O., Soriano-Navarro, M., Zamora-Berridi, G., García-Verdugo, J.M., and Quinoñes-Hinojosa, A. (2011). Cytoarchitecture of the lateral ganglionic eminence and rostral extension of the lateral ventricle in the human fetal brain. J. Comp. Neurol. *519*, 1165-1180.

Gundersen, G.G., and Worman, H.J. (2013). Nuclear positioning. Cell *152***,** 1376-1389.

Hering, H., and Sheng, M. (2001). Dendritic spines: Structure, dynamics and regulation. Nature Rev. Neurosci. Vol 2.

Suh, H., Consiglio, A., Ray, J., Sawai, T., D'Amour, K. A, and Gage, F. H. (2007). In vivo fate analysis reveals the multipotent and self-renewal capacities of Sox2+ neural stem cells in the adult hippocampus. Cell Stem Cell *1*,515-28.

Jones, J., Estirado, A., Redondo, C., Bueno, C., and Martínez S. (2012). Human adipose stem cell-conditioned médium increases survival of friedreich`s ataxia cells submitted to oxidative stress. Stem Cells Dev. *21*, 2817-2826.

Kuhn, H.G., Dickinson-Anson, H., and Gage F.H. (1996). Neurogenesis in the dentate gyrus of the adult rat: Age-Related decrease of neuronal progenitor proliferation. J. Neurosci. *16*, 2027-2033.

Kuhn, H.G., Eisch, A.J., Spalding, K., and Peterson, D.A. (2016). Detection and Phenotypic Characterization of Adult Neurogenesis. Cold Spring Harb. Perspect. Biol. 8(3):a025981.

Liu, J.A., and Cheung, M. (2016). Neural crest stem cell and their potential therapeutic applications. Dev. Biol. *419*, 199-216.

Merriam, E.B., Millette, M., Lumbard, D.C., Saengsawang, W., Fothergill, T., Hu, X., Ferhat, L., and Dent, E.W. (2013). Synaptic regulation of microtubule dynamics in dendritic spines by calcium, F-actin, and debrin. J. Neurosci. *33*, 164711-164782.

Palmer, T.D., Ray, J., and Gage, F.H. (1995). FGF-2-responsive neuronal progenitors reside in proliferative and quiescent regions of the adult rodent brain. Mol. Cell Neurosci. *6*, 474-486.

Powell, S.K., Rivas, R.J., Rodriguez-Boulan, E., and Hatten, M.E. (1997). Development of polarity in cerebellar granule neurons. J. Neurobiol. *32*, 223-236.

Quesada, M.P., Jones, J., Rodríguez-Lozano, F.J., Moraleda, J.M., and Martinez, S. (2015). Novel aberrant genetic and epigenetic events in friedreich´s ataxia. Exp. Cell Res. *335*, 51-61.

Reynolds, B. A., and Weiss, S. (1992). Generation of neurons and astrocytes from isolated cells of the adult mammalian central nervous system. Science *255*:1707-10.

Ros, O., Cotrufo, T., Martinez-Marmol, R., and Soriano, E. (2015). Regulation of patterned Dynamics of local exocytosis in growth cone by netrin-1. J. Neurosci. *13*, 5156-5170.

Seri, B., Garcia-verdugo, J.M., McEwen, B.S., and Alvarez-buylla, A. (2001). Astrocytes give rise to new neurons in the adult mammalian hippocampus. J. Neurosci. *21*, 7153-7160.

Seri, B., Garcia-verdugo, J.M., Collado-Morente, L., McEwen, B.S., and Alvarez-buylla, A. (2004). Cell types, lineage, and architecture of the germinal zone in the adult dentate gyrus. J. Com. Neurol. *474*, 359-378.

Skinner, B.M., and Johnson, E.E. (2017). Nuclear morphologies: their diversity and functional relevance. Chromosoma. *126*, 195-212.

Sohur, U.S., Emsley, J.G., Mitchell, B.D., and Macklis, J.D. (2006). Adult neurogenesis and cellular brain repair with neural progenitors, precursors and stem cells. Philos. Trans. R. Soc. Lond. B. Biol. Sci. *361*, 1477-1497.

Tahirovic, S., and Bradke, F. (2009). Neuronal polarity. Cold Spring Harb. Perspect. Biol. vol. 1, no. 3.

Takano, T., Xu. C., Funahashi, Y., Namba, T., and Kaibuchi K. (2015). Neuronal polarization. Development *142*, 2088-2093.

Uberti, D., Ferrar-Toninelli G., and Memo, M. (2003). Involvement of DNA damage and repair systems in neurodegenerative process. Oxicol. Lett. *139*, 99-105.

Urbach, A., Redecker, C., and Witte, O.W. (2008). Induction of neurogenesis in the adult dentate gyrus by cortical spreading depression. Stroke. *39*, 3064-3072.

Van Oijen, M.G., Medema, R.H., Slootweg, P.J., and Rijksen, G. (1998). Positivity of the proliferation marker Ki-67 in noncycling cells. Am. J. Clin. Pathol. *110*, 24-31.

Von Bohlen Und Halbach O. (2009). Structure and functions of dendritic spines. Ann. Anat. *191*, 518-531.

Figure legends

Figure 1. Morphological changes in hPDLSCs cultures during neural induction. (A and B) Undifferentiated hPDLSCs presented a fibroblast-like morphology with low-density microvilli on their surface (A) and actin microfilaments and β-III tubulin microtubules oriented parallel to the longitudinal axis of the cell (B). (C) Western blot analysis verified the expression of β-III tubulin. Protein size markers (in kilodaltons) are indicated on the side of the panel. (D). Undifferentiated hPDLSCs displayed a flattened, ellipsoidal nucleus often located in the center of the cell. (E) After 14 days of neural differentiation conditions, hPDLSCs with different morphologies were observed. (F) In addition, hPDLSCs of various size were also observed. (G) Microscopic analysis also revealed that some hPDLSCs have different nuclear size and shapes, including segmented nuclei connected by an internuclear bridge. Scale bar: 25 μm. SEM, scanning electron microscopy; LM, light microscopy.

Figure 2. *In vitro* neurogenesis from hPDLSCs. (A) After neural induction, hPDLSCs undergo a shape and size change, adopting highly irregular forms first and then gradually contracting into round cells. (B) Cytoskeletal remodeling is observed during these morphological changes. Actin microfilament not longer surround the nucleus and become cortical. Unlike actin, β-III tubulin seems to accumulate around the nucleus. (C) the cytoskeletal network is almost lost in round cells. (D) Scanning electron micrographs show that there is a marked increase in the density of microvilli as the cells round up to near-spherical shape. (E) The surface of round cells is almost devoid of microvilli. The escale bars are 25 μm in the light microscope images, and 10 μm in the scanning electron micrographs. LM, light microscopy; SEM, scanning electron microscopy.

Figure 3. Neuronal polarization of hPDLSCs-derived neurons. (A) hPDLSCs-derived neurons start their development as rounded spheres that initiate neurite outgrowth at a single site on the plasma membrane. (B) These later transform into cells containing several short neurites developed around the cell body. (C) the cytoskeletal network is reorganizated. β-III tubulin

accumulates densely under the cellular membrane of the cell body and in cell neurites while actin microfilaments are mainly found in cell neurites. (D) The peripheral domain in the growth cone of hPDLSCs-derived neurons is composed of radial F-actin bundles and the central domain contains β-III tubulin microtubules. (E) Micrographs showing that the growth cone also contains filopodia and vesicles on the cell surface. (F and G) At later stages of development, hPDLSCs-derived neurons gradually adopt a complex morphology (F) giving rise to a variety of neuron-like forms (G). (H) Cytoskeletal protein β-III tubulin and F-actin staining shown that hPDLSCs-derived neurons develop distinct axon-like and dendrite-like processes (numbers locate the areas shown in higher power). The escale bars are 25 μm in the light microscope images, and 10 μm in the scanning electron micrographs. SEM, scanning electron microscopy; LM, light microscopy; b, actin bundles; v, vesicles, f, filopodia.

Figure 4. hPDLSCs-derived neurons have developed well-differentiated axonal-like and dendritic-like domains. (A) Scanning electron micrographs show that hPDLSCs-derived neurons are composed of multiple branched processes with different spine-like protusions highly similar to filopodium, mushroom, thin, stubby, and branched dendritic spines shapes. (B-D) hPDLSCs-derived neurons also display different types of axonal branch-like structures, including bifurcation (B), terminal arborization (C), and collateral formation (D) (inserts and numbers locate the areas showed in higher power). The escale bars are 25 μm in light microscope images and 5 μm in the scanning electron micrographs. SEM, scanning electron microscopy; LM, light microscopy; s, spine-like protusions; f, filopodium; m, mushroom; t, thin; stubby; b, branched. B, bifurcation; a, arborization; c, collateral formation.

Figure 5. hPDLSCs-derived neurons are connected by synapse-like interactions. (A and B) hPDLSCs-derived neurons connect to one another (A) through different types of synapses-like interactions, including dendrodendritic-like, axoaxonic-like and axodendritic-like synapses (B). (C) Synapse-associated proteins Cx43, Synaptophysin and Synapsin1 are found in the cell membrane of hPDLSCs-derived neurons at the neurite contact areas. Scale bar: 25 μm. LM, light microscopy; DD, dendrodendritic-like synapse; AA, axoaxonic-like and synapse; AD, axodendritic-like synapse.

Figure 6. Nuclear shape remodeling occurs during neurogenesis from hPDLSCs. (A-I) The nucleus located in the center of the cell starts to move towards an asymmetrical position within the cell. (J-Z) This nucleus movement is accompanied by the transient formation of segmented nuclei connected by an internuclear bridge (J-T). Finally, there is restoration of the irregular, but non-segmented, nucleus with an eccentric position within PDL-derived neurons (U-Z). The escale bars in β-III tubulin and DAPI images are 50 μm and 10 μm for confocal 3D images of nuclei.

Figure 7. Neurogenic niches in the adult mammalian brain also contains cells with irregular nuclei. (A and B) Morphological analysis reveals that the adult rodent V-SVZ of the anterolateral ventricle wall (A), as well as the SGZ of the hippocampal dentate gyrus (B), contain cells with

nuclear shapes highly similar to those observed in during *in vitro* neurogenesis from hPDLSCs. Scale bar: 10 μm. LV, lateral ventricle; GLC, granule cell layer.

Figure S1. Nuclear shape in PDL-derived neurons. (A) No segmented nuclei are observed when PDL-derived neurons gradually acquired cellular polarity and more mature, neuronal-like morphology. (B) The nuclear volume shrinks as the cells become rounded during neurogenesis. Data represent mean ± S.E. of ten independent experiments. The escale bar in β-III tubulin and DAPI images are 50 μm and 10 μm for confocal 3D images of nuclei.

Methods

Ethical approval. Methods were carried out in accordance with the relevant guidelines and regulations. The experimental protocols were approved by the Institutional Review Board of the Miguel Hernández University of Elche (No. UMH.IN.SM.03.16) and the informed consent was obtained from all patients before the study.

Cell Culture. Human premolars were extracted and collected from normal adult patients undergoing orthodontic therapy in Murcia dental hospital (Spain). hPDL was scraped from the middle third region of the root surface. After washing the extracted PDL with Ca and Mg-free Hank's balance salt solution (HBSS; Gibco), hPDL was digested with 3 mg/ml type I collagenase (Worthington Biochemical Corporation) and 4 mg/ml dispase II (Gibco) in alpha modification minimum essential medium eagle (α-MEM) (α-MEM; Sigma-Aldrich) for 1 h at 37°C. The reaction was stopped by the addition of α-MEM. The dissociated tissue was passed through a 70-μm cell strainer (BD Falcon). Cells were centrifuged, and the pellet was resuspended in in serum-containing media (designated as the basal media), composed of α-MEM supplemented with 15% calf serum (Sigma), 100 units/ml penicillin-streptomycin (Sigma) and 2 mM l-glutamine (Sigma). The cell suspension was plated into six-well multiwell plates (BD Falcon) and incubated at 37°C in 5% CO2. To induce neural differentiation, cells were cultured in serum-free media (designated as the neural induction media), consisting in Dulbecco's modified Eagle's medium/F12 (DMEM/F12, Gibco) supplemented with bFGF (20 ng/ml, R&D Systems), EGF (20 ng/ml, R&D Systems), glucose (0.8 mg/ml, Sigma), N2-supplement (Gibco), 2 mM l-glutamine (Sigma), and 100 units/ml penicillin-streptomycin (Sigma). Neural induction media were changed every 3-4 days until the end of the experiment (2 weeks).

Immunocytochemistry. Cells were plated onto poli-L-lysine (10 μg/ml, Sigma-Aldrich) coated plastic or glass coverslips, and maintained in basal media or neural induction media. Cells were rinsed with PBS and fixed in freshly prepared 4% paraformaldehyde (PFA; Sigma). Fixed cells were blocked for 1 h in PBS containing 10% normal horse serum (Gibco) and 0.25% Triton X-100 (Sigma) and incubated overnight at 4°C with antibodies against: β-III-tubulin (TUJ1; 1:500, Covance), Conexin 43 (3512; 1/300, Cell Signalling), Synaptophysin (18-0130; 1/300, Zymed)

and Synapsin1 (NB300-104; 1/300, Novus) in PBS containing 1% normal horse serum and 0.25% Triton X-100. On the next day, cells were rinsed and incubated with the corresponding secondary antibodies: Alexa Fluor® 488 (anti-mouse or anti-rabbit; 1:500, Molecular Probes), Alexa Fluor® 594 (anti-mouse or anti-rabbit; 1:500, Molecular Probes), biotinylated anti-rabbit (BA1000, 1:250; Vector Laboratories), biotinylated anti-chicken (BA9010, 1:250, Vector Laboratories, CY3-streptavidin (1:500, GE Healthcare). Cell nuclei were counterstained with DAPI (0.2 mg/ml in PBS, Molecular Probes). Alexa Fluor 488® phalloidin was used to selectively stains F-actin (Molecular Probes)**.**

Western Blotting. hPDL-derived cells were harvested using trypsin/EDTA (Gibco), washed twice with PBS, resuspended in RIPA lysis buffer (Millipore) for 30 min at 4°C in the presence of protease inhibitors (Pierce™. protease inhibitor Mini Tables, Pierce Biotechnology Inc) and PMSF 1M (Abcam). Protein concentration was determined using the bradford protein assay (Sigma-Aldrich). Proteins were separated in 8% SDS-polyacryamide gel (PAGE-SDS) and transferred to a nitrocellulose membrane (Whatman). PageRuler™ Prestained Protein Ladder (Thermo Scientific) has been used as size standards in protein electrophoresis (SDS-PAGE) and western-blotting. After transfer, nitrocellulose membranes were stained with Ponceau S solution (Sigma-Aldrich) to visualize protein bands. Blots were then incubated over-night at 4°C with rabbit antibody against β-III-tubulin (TUJ1; 1:1000, Covance). Secondary antibody was used at 1:7000 for peroxidase anti-mouse Ab (PI-2000, Vector Laboratories). Immunoreactivity was detected using the enhanced chemiluminescence (ECL) Western blot detection system (Amersham Biosciences Europe) and Luminata™ Forte (Millipore corporation) using ImageQuant *LAS 500* Gel Documentation System (GE Healthcare). The molecular weight of b-III-tubulin is approximately 55 kDa.

Immunohistochemistry. Experiments were carried out according to the guidelines of the European Community (Directive 86/609/ECC) and in accordance with the Society for Neuroscience recommendations. Animals used in this study were 12-week-old immune-suppressed mouse (Hsd:Athymic Nude-Foxn1 nu/nu; Harlan Laboratories Models, S.L), housed in a temperature and humidity controlled room, under a 12h light/dark cycles, with *ad libitum* access to food and water. The animals were anesthetized with an overdose of chloral hydrate and intracardially perfused with freshly prepared, buffered 4% PFA (in 0.1M PB, pH 7.4). Brains were removed, post-fixed for 12 hr in the same fixative at 4ºC and dehydrated in 30% sucrose solution at 4°C until sunk. 30µm thick coronal sections were collected using a freezing microtome. Serial sections were used for DAPI staining. Free-floating sections were incubated and mounted onto Superfrost Plus glass slides (Thermo Scientific). The slides were dried O/N and coverslipped with mowiol-NPG (Calbiochem).

Images and data analyses. Analyses and photography of visible and fluorescent stained samples were carried out in an inverted Leica DM IRB microscope equipped with a digital camera Leica DFC350FX (Nussloch) or in confocal laser scanning microscope Leica TCS-SP8. Digitized

images were analyzed using LASX Leica confocal software. Z-stacks of confocal fluorescent images were also analyzed to calculate the nuclear volume by using ImageJ software.

Scanning electron microscopy. Cells were plated onto poli-L-lysine (10 µg/ml, Sigma-Aldrich) coated glass coverslips and maintained in basal media or neural induction media. Cells were treated with fixative for 20 minutes. Coverslips were postfixed in 1% osmium tetroxide for 1 hour and dehydrated in graded ethanol washes. The coverslips were allowed to dry at a conventional critical point and were then coated with gold-palladium sputter coated. Coverslips were view on a Jeol 6100 scanning electron microscope.

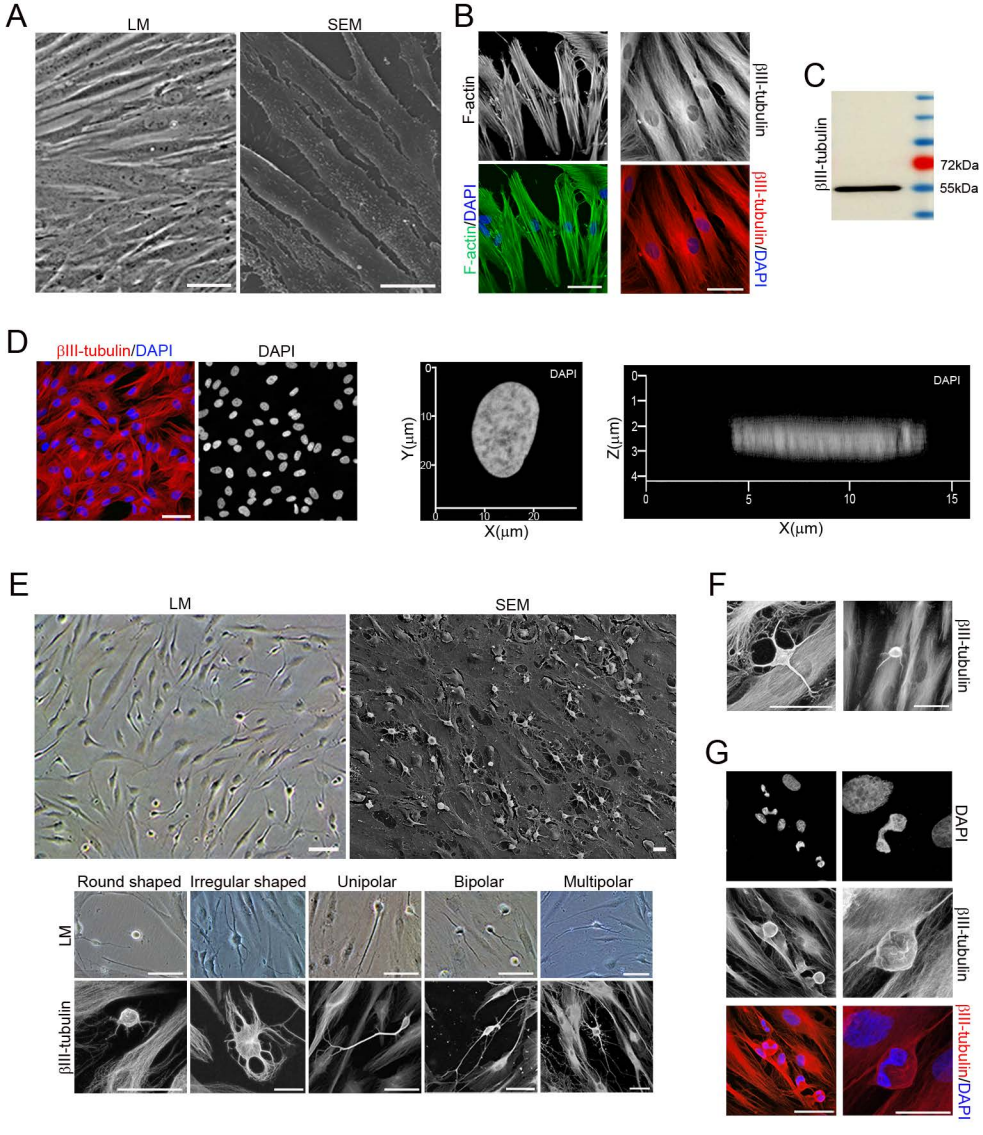
A
LM
SEM
B
F-actin
βIII-tubulin
F-actin/DAPI
βIII-tubulin/DAPI
C
βIII-tubulin
72kDa
55kDa
D
βIII-tubulin/DAPI
DAPI
DAPI
Y(μm)
X(μm)
DAPI
Z(μm)
X(μm)
E
LM
SEM
Round shaped
Irregular shaped
Unipolar
Bipolar
Multipolar
LM
βIII-tubulin
F
βIII-tubulin
G
DAPI
βIII-tubulin
βIII-tubulin/DAPI

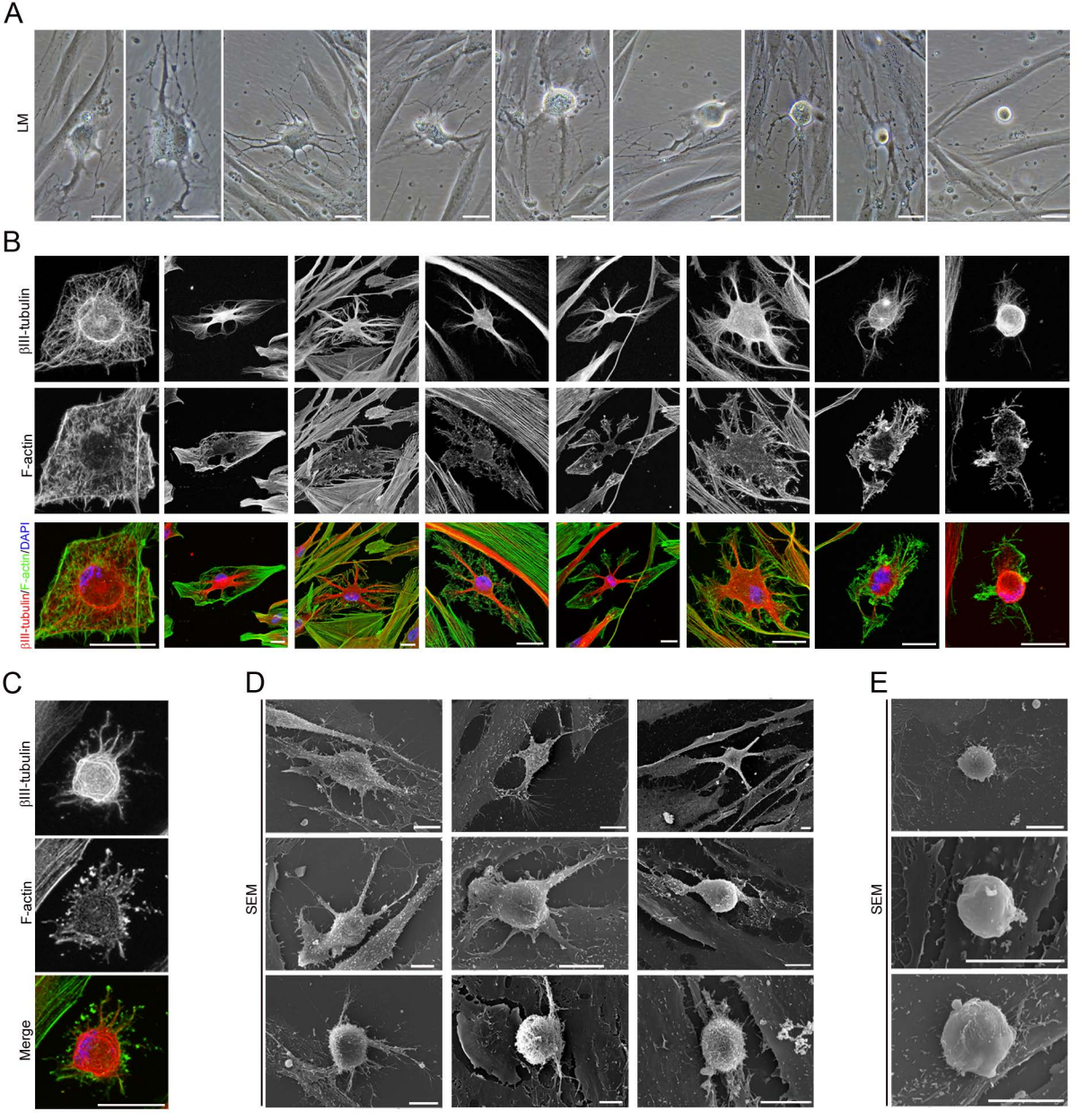
A
LM
B
βIII-tubulin
F-actin
βIII-tubulin/F-actin/DAPI
C
βIII-tubulin
F-actin
Merge
D
SEM
E
SEM

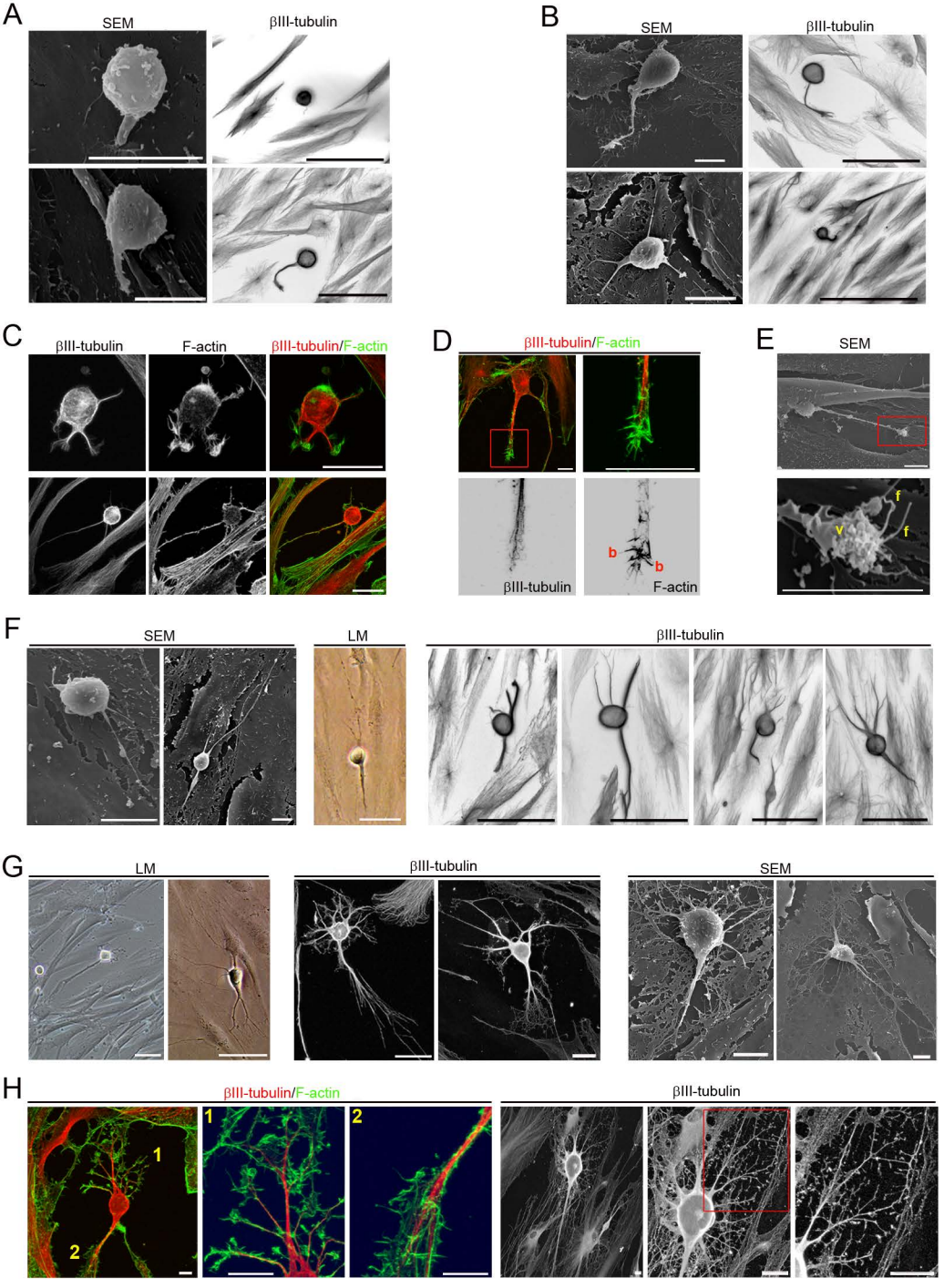
A
SEM
βIII-tubulin
B
SEM
βIII-tubulin
C
βIII-tubulin
F-actin
βIII-tubulin/F-actin
D
βIII-tubulin/F-actin
b
b
βIII-tubulin
F-actin
E
SEM
f
v
f
F
SEM
LM
βIII-tubulin
G
LM
βIII-tubulin
SEM
H
βIII-tubulin/F-actin
1
2
1
2
βIII-tubulin

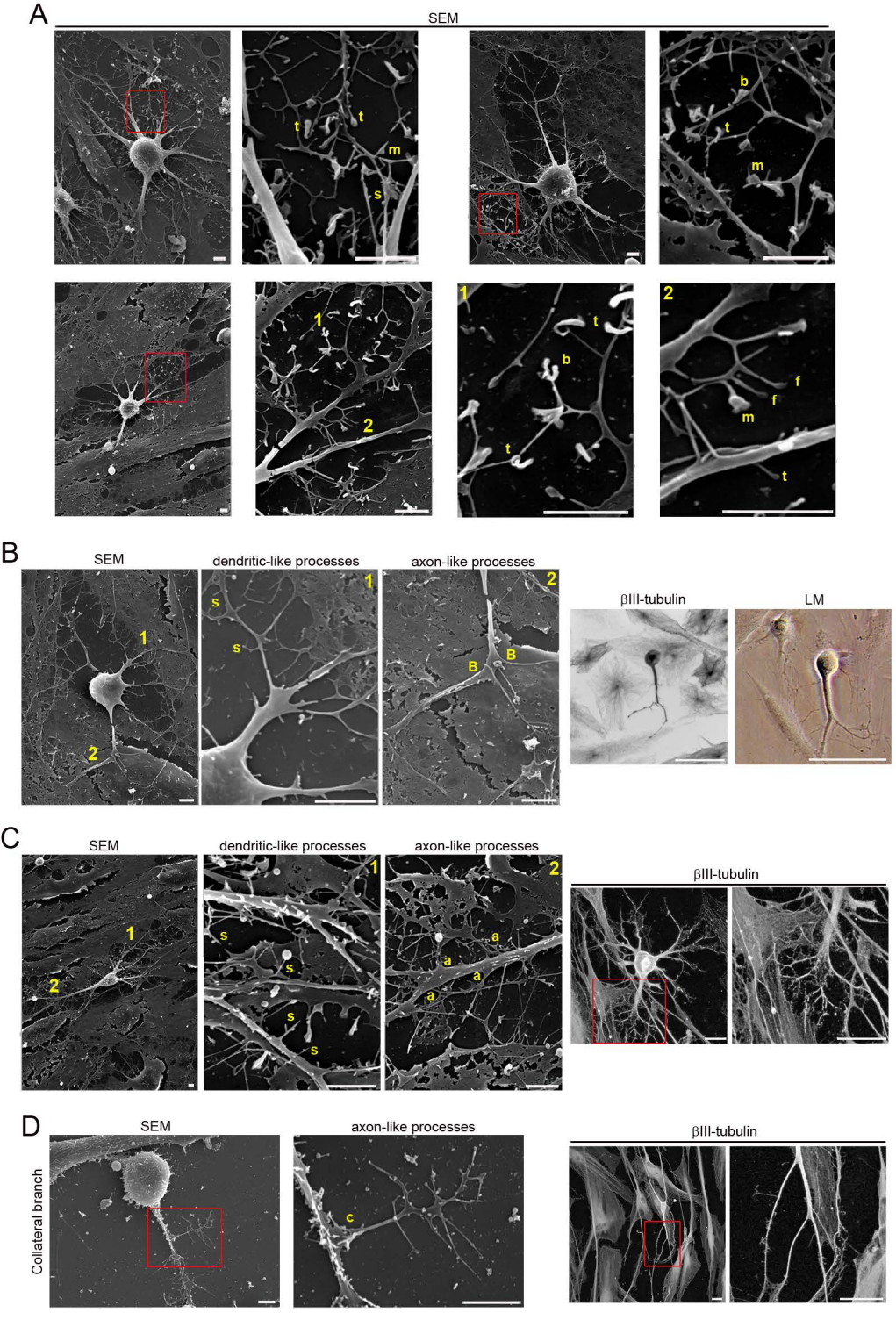
A
SEM
t
t
m
s
b
t
m
1
2
1
t
b
t
2
f
f
m
t
B
SEM
dendritic-like processes
axon-like processes
1
2
s
s
1
B
B
2
βIII-tubulin
LM
C
SEM
dendritic-like processes
axon-like processes
1
2
s
s
s
s
1
a
a
a
a
2
βIII-tubulin
D
SEM
axon-like processes
βIII-tubulin
Collateral branch
c

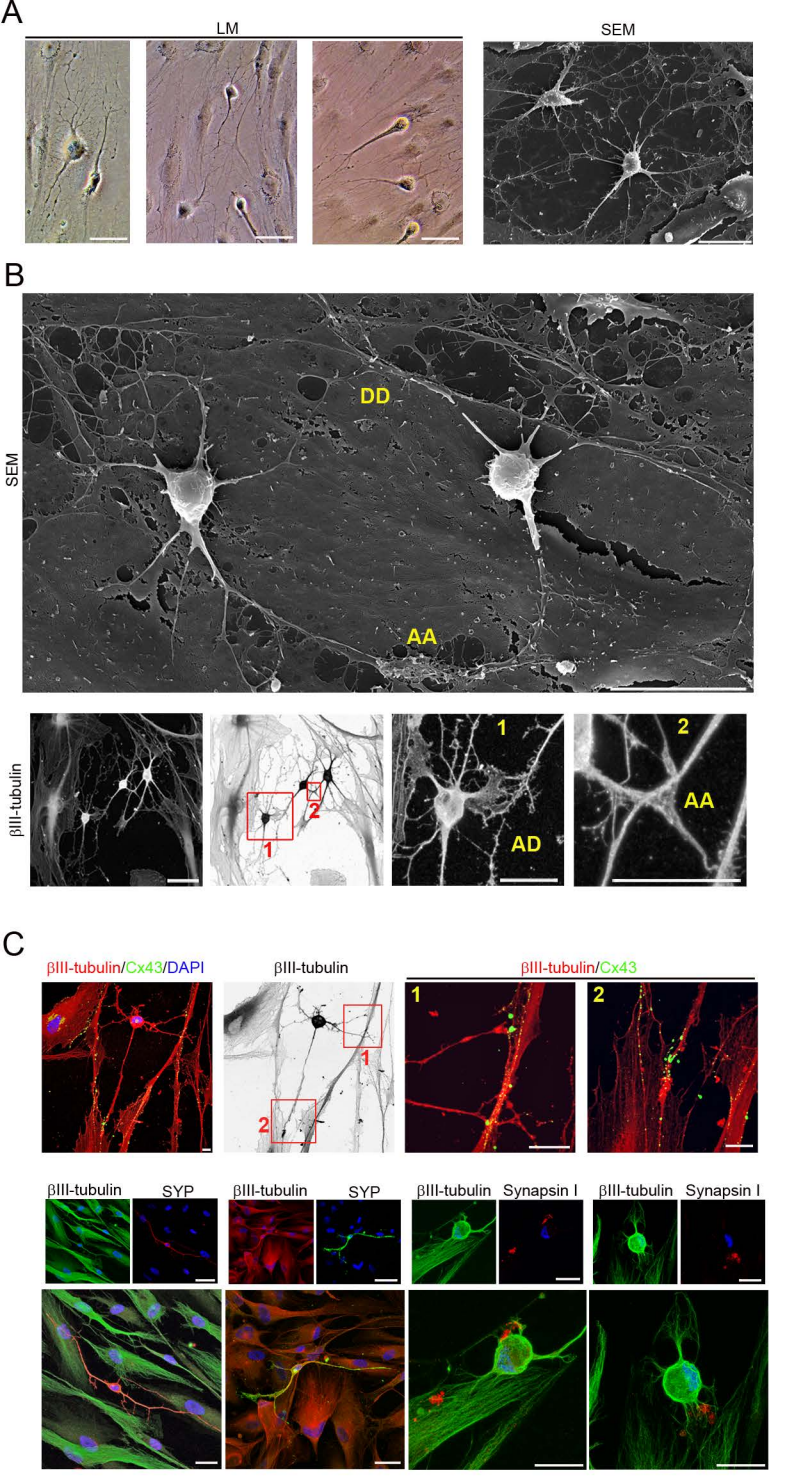
A
LM
SEM
B
SEM
DD
AA
βIII-tubulin
1
2
1
AD
2
AA
C
βIII-tubulin/Cx43/DAPI
βIII-tubulin
βIII-tubulin/Cx43
1
2
1
2
βIII-tubulin
SYP
βIII-tubulin
SYP
βIII-tubulin
Synapsin I
βIII-tubulin
Synapsin I

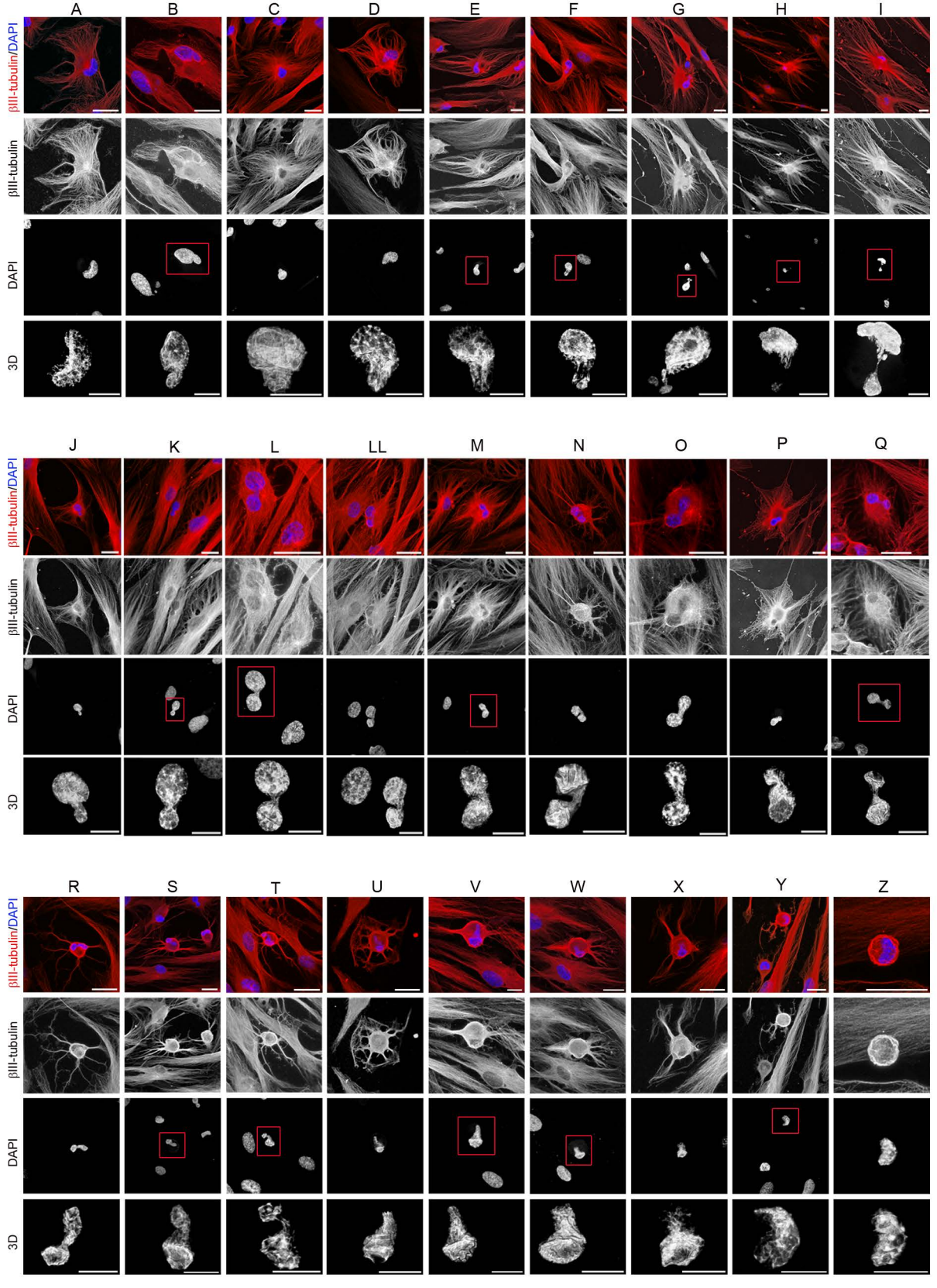
A
B
C
D
E
F
G
H
I
βIII-tubulin/DAPI
βIII-tubulin
DAPI
3D
J
K
L
LL
M
N
O
P
Q
βIII-tubulin/DAPI
βIII-tubulin
DAPI
3D
R
S
T
U
V
W
X
Y
Z
βIII-tubulin/DAPI
βIII-tubulin
DAPI
3D

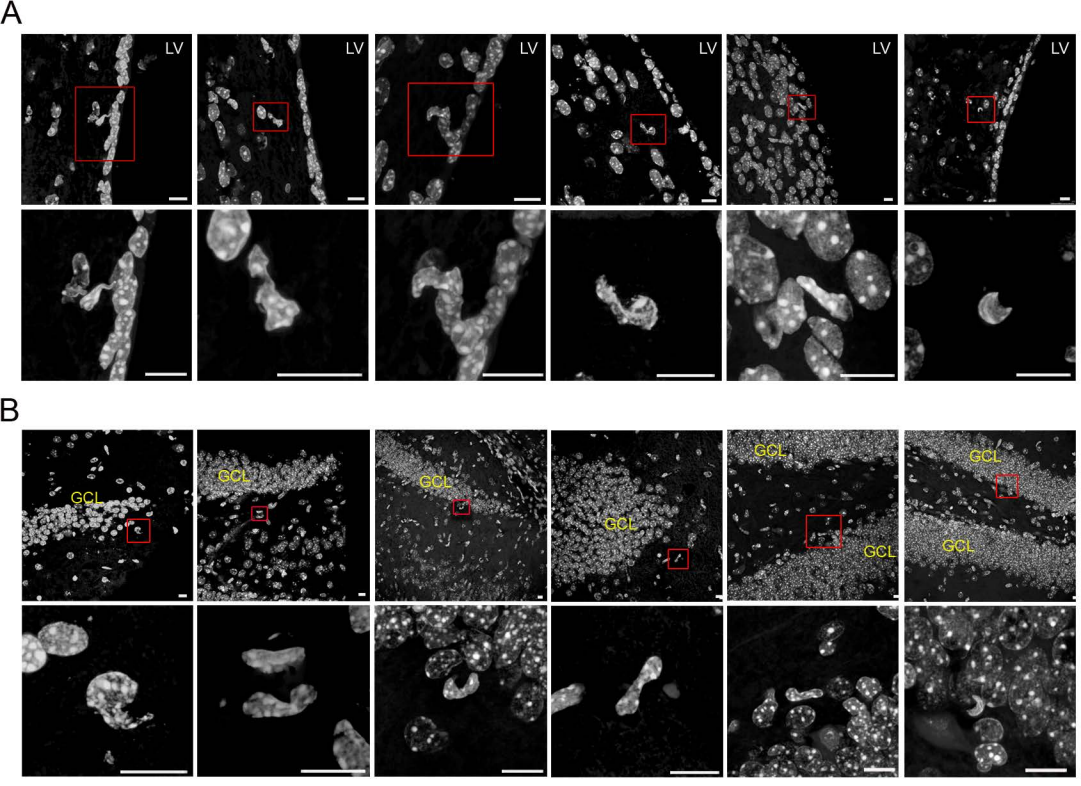
A
LV
LV
LV
LV
LV
LV
B
GCL
GCL
GCL
GCL
GCL
GCL
GCL

A

βIII-tubulin/DAPI

βIII-tubulin

DAPI

3D
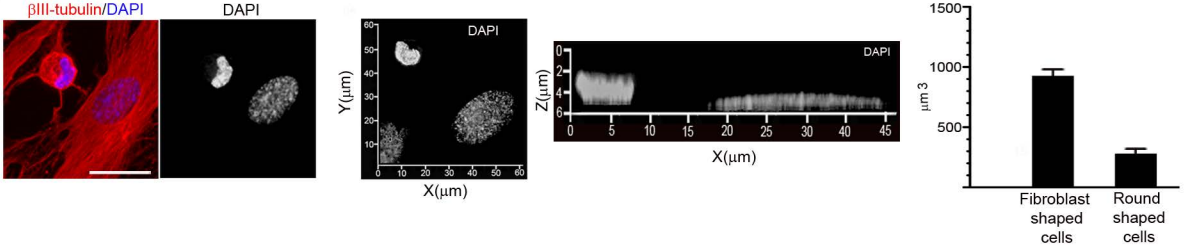
B